Materials and Design 60 (2014) 605–611

Contents lists available at ScienceDirect

Materials and Design

journal homepage: www.elsevier.com/locate/matdes

Effect of carbon on the density, microstructure and hardness of alloys formed by mechanical alloying

Wilbert David Wong-Ángel [a,*], Lucia Téllez-Jurado [a], Elizabeth Chavira-Martínez [b], José Federico Chávez-Alcalá [a], Enrique Rocha-Rangel [c]

[a] Instituto Politécnico Nacional-ESIQIE, Depto. Ing. Metalurgia y Materiales, Zacatenco, C.P. 07738, México D.F., Mexico
[b] Universidad Nacional Autónoma de México, Instituto de Investigaciones en Materiales, A.P. 70-360, C.P. 04510 México D.F., Mexico
[c] Universidad Politécnica de Victoria, Avenida Nuevas Tecnologías 5902, Parque Científico y Tecnológico de Tamaulipas, C.P. 87137, Ciudad Victoria, Tamaulipas, Mexico

ARTICLE INFO

Article history:
Received 20 January 2014
Accepted 11 April 2014
Available online 21 April 2014

Keywords:
Mechanical alloying
Pressing
Sintering
Hardness
Density

ABSTRACT

This work aimed to produce iron-based alloys containing resistant microstructures to improve the mechanical properties of the resulting alloy. The effects of both carbon content and compaction pressure on the microstructure, density and hardness of the alloys were examined. Iron-based alloys with initial carbon contents of 0.5%, 1%, 2% and 3% were produced by powder metallurgy following a process that involved ball milling elemental powders, cold pressing and sintering. The composition, density, microstructure, porosity, hardness and ductility of the alloys depended on both compaction pressure and carbon content. As the carbon content increased, the amount of the resistant microstructure bainite in the alloys also increased, as did their hardness. In contrast, the density and ductility of the alloys decreased with increasing carbon content. This study shows that formation of the resistant microstructure bainite in alloys fabricated by powder metallurgy is influenced by both the initial carbon content of the alloy and compaction pressure during cold pressing.

1. Introduction

Iron-based alloys are widely used in vehicle, marine, aviation, structural and power tool components because of their high strength in relation to their cost [1,2]. Powder metallurgy (PM) is a well-established technique that allows alloys to be produced from solid-state samples [3]. Alloys with complex geometries can be prepared, which reduces secondary machining and thus cost, and makes PM competitive with other alloy formation processes [4]. Another advantage of PM is that it can be used to produce resistant microstructures such as tempered martensite and bainite that can withstand large stresses and improve the mechanical properties of the resulting alloy [5].

However, the alloys obtained by PM contain pores, which can induce cracks that may propagate through the alloy [6]. The porosity of alloys formed by PM is in the order of 5–15%, and depends on the compressibility of the alloying powders, amount of carbon and lubricant added to the iron powder base [7]. A heterogeneous porosity distribution in an alloy damages its mechanical properties [8]. To prevent this, resistant microstructures can be formed in steel by adding small quantities of alloying elements to compensate for the microcracks formed by the pores [9]. The interaction of carbon and alloying elements (Cr, Mo, Si and Mn) with dislocations and substitutions of atoms have a substantial effect on the mechanical properties of the resulting alloy. Addition of Cr improves the mechanical properties of sintered steel through solution hardening and carbide precipitation, while addition of Mo promotes formation of bainitic microstructure [10,11].

Carbon is one of the most frequent interstitial atoms in the steel matrix and affects its hardness, density and crystal structure [12]. Bensebaa et al. [13] found that the formation of ferrite nanocrystals with a high carbon content improved the properties of steel. Lonardelli et al. [14] prepared medium carbon steel containing bainitic structure by PM and examined its mechanical properties and thermal stability. They found that samples with a higher carbon content showed reduced thermal stability.

The properties of steels are also affected by processing parameters such as compaction pressure. In a theoretical study, Azadbeh et al. [15] found that compaction pressure strongly influenced the properties of Cr–Mo prealloyed sintered steels because it determined the interparticle contact area. Optimal transverse rupture strength, hardness, and impact energy were calculated for a

* Corresponding author. Tel.: +52 (55)57296000x54209; fax: +52 (55) 57296000x54268.
E-mail address: wwonga0900@alumno.ipn.mx (W.D. Wong-Ángel).

http://dx.doi.org/10.1016/j.matdes.2014.04.039
0261-3069/

compaction pressure of 700 MPa. Meanwhile, Channankaiah and Ranganath [1] found that the density of AISI 4140 steel increased with compaction pressure until it became saturated at about 450 MPa. They also found that the aspect ratio of the preform and homogenization time influenced density and mechanical properties.

In this work, Fe-based alloys by PM containing different carbon contents were prepared in order to examine the effect of carbon content on the density, microstructure and mechanical properties of the alloys with the aim of forming resistant microstructures. Alloys containing 0.5%, 1%, 2% and 3% C in 1% Mn, 0.25% Mo, 0.3% Si, 1.1% Cr and the balance Fe (hereafter referred to as 0.5%, 1%, 2% and 3% C alloys, respectively) are prepared by mechanical alloying followed by compaction and sintering. The alloys are compacted at different pressures in the range of 100–600 MPa to examine the effect of compaction pressure on their density, microstructure and hardness. Material hardness is influenced by carbon content because it changes the microstructure of the sample. With increasing carbon content, the hardness and tenacity of the samples increase and decrease, respectively.

2. Experimental details

Iron (Aldrich, 99.9%, <10 μm), chromium (Aldrich, 99%, <43 μm), molybdenum (Aldrich, 99.9%, 1–2 μm), silicon (Aldrich, 99%, <10 μm), manganese (Aldrich, 99.9%, <43 μm) and carbon (Aldrich, 99.99%, <43 μm) powders were used as starting materials. Each powder was accurately weighed using an analytical balance with an error of ±0.0001 g. Each mixture was ground for 48 h using a custom-built horizontal stainless steel ball mill 15.2 cm in length and 12.5 cm in diameter containing balls of hardened steel (carburized AISI 1010 steel) with a ball load of 2461 g and ball/powder weight ratio 36:1. Stearate acid (0.8 wt%) was used as a control agent in the milling process. The chamber was filled with 200 kPa of high-purity Ar gas during milling to prevent oxidation of exposed surfaces.

After milling, each powder (10 g) was compacted at 100–600 MPa and velocity of 40 mm s^{-1} using a hydraulic press (Rps200, Lauffer, capacity of 200 tons) to obtain a pellet with a diameter of 22 mm and thickness of 10 mm. The green density of each pellet was measured using a bushing-type exterior micrometer (0–25 mm, resolution: 0.001 mm, Model 293, Mitutoyo America Co., Aurora, USA). Green pellets were sintered in a continuous furnace (GmbH High Temperature Sintering Furnace, MAHLER, Plochingen, Germany) under a flow of reducing gas at 500 °C for 40 min and then at 1200 °C for 35 min with a heating rate of 10 °C min^{-1}. The density of the sintered particles was measured according to Metal Powder Industries Federation Standard 42 [16].

Table 1
Post-milling compositions of alloys with different initial carbon contents.

Element (%)						
Initial C	Final C	Mn	Mo	Si	Cr	Fe
0.5	0.68	1.16	0.36	0.41	1.40	95.99
1.0	1.09	1.18	0.32	0.38	1.25	95.78
2.0	2.08	1.13	0.29	0.39	1.15	94.99
3.0	3.11	1.15	0.33	0.37	1.21	93.83

The microstructure of the alloys was observed with an optical microscope (Axio Visio, Carl Zeiss, Germany) and scanning electron microscope (SEM, JSM 6490, JEOL, Japan). Samples were polished and etched with 2% natal before observation. Sample hardness was measured with a Vickers microhardness tester (HM 112, Mitutoyo, Japan) using a diamond indenter with a load of 100 g for 8 s. Powder X-ray diffraction (XRD) measurements were obtained on a diffractometer (D8 Focus, Bruker, Germany) at a voltage of 35 kV, current of 25 mA and scan velocity of 2° min^{-1}.

After power ball milling for 48 h, samples for impact experiments were prepared by compacting each powder (60 g) in a steel mold using the same hydraulic press at a pressure of 500 MPa to give samples with a cross section of 12 mm × 12 mm and length of 600 mm. Samples were sintered in a continuous furnace (Mahler) and machined to obtain Charpy-type samples with dimensions of 5 mm × 10 mm × 55 mm according to ASTM: E-23-12c. Standard Charpy impact tests were carried out using a pendulum Izod impact test apparatus and a Charpy impact testing machine (model JBW-300, PTE, Shandong, China). Transmission electron microscope (TEM) characterization of the sintered samples was performed using a TEM (2000FX, JEOL, Tokyo, Japan), operating at 200 kV equipped with an energy-dispersive spectrometer (EDS) and also by high-resolution TEM (HRTEM, 2100, JEOL, Tokyo, Japan), operating at 200 kV, using a LaB_6 filament.

3. Results and discussion

Representative SEM images of the 2% C alloy showing its morphology after milling are presented in Fig. 1. The milled alloy is composed of flakes. The overall compositions of the alloys after milling are given in Table 1; each is similar to the nominal composition of the corresponding sample. The elemental distribution of the 2% C alloy after milling is presented in Fig. 2. All of the elements are relatively well distributed through the alloy, although some particles of CrFe and CrFeMn are observed. These results are consistent with those of Arik and Turker [17], who achieved a homogeneous distribution of Fe_3C particles in the matrix by high-energy mechanical alloying. The other alloys contained

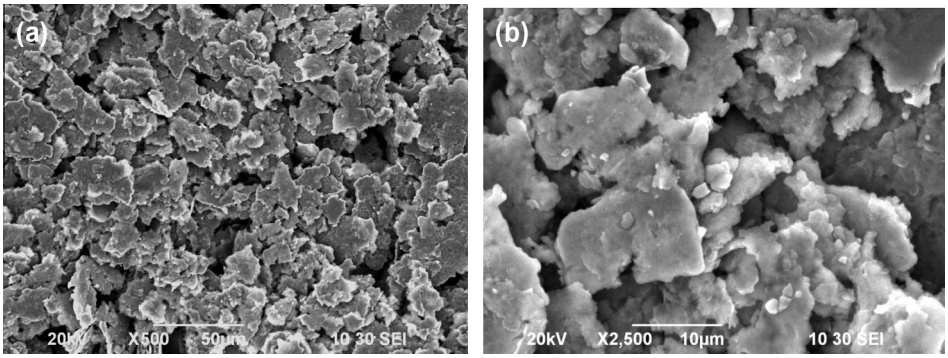

Fig. 1. SEM micrographs of 2% C alloy at a magnification of (a) ×600 and (b) ×2500.

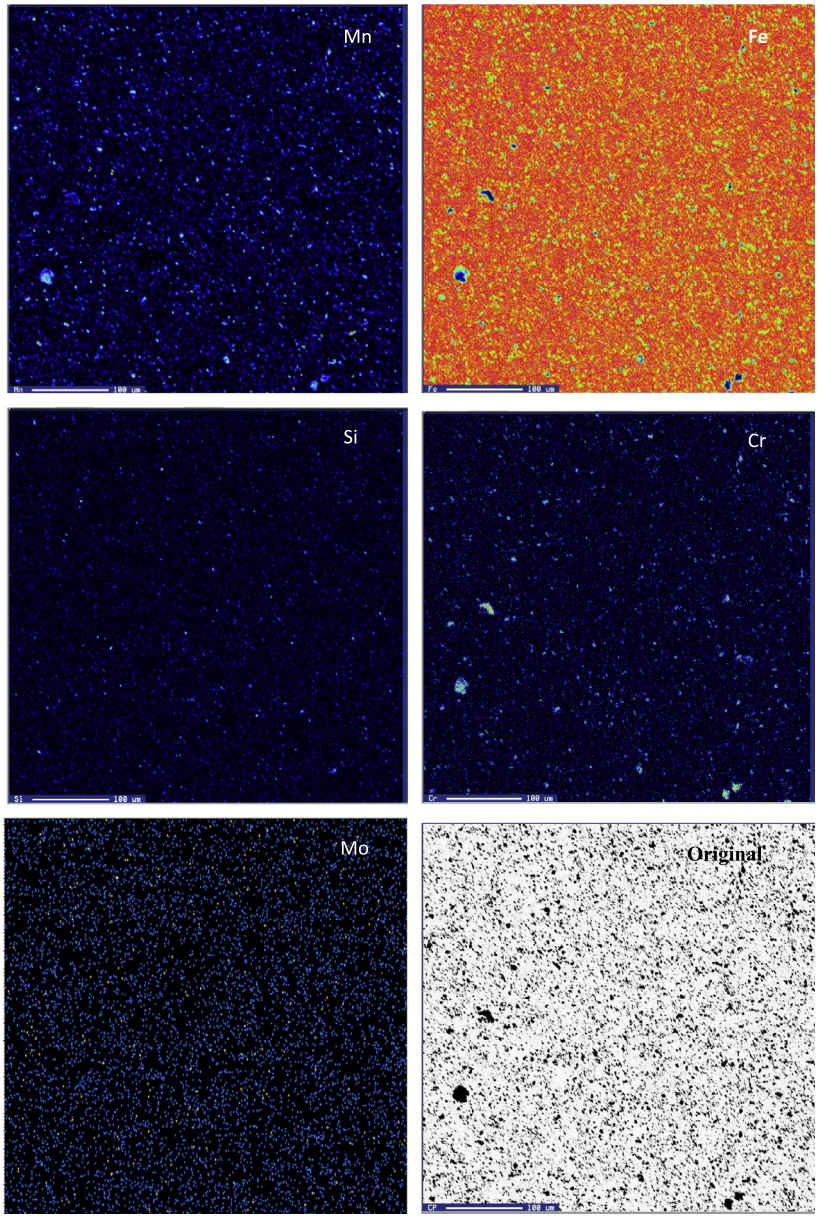

Fig. 2. Optical micrographs showing the elemental distribution in the 2% C alloy.

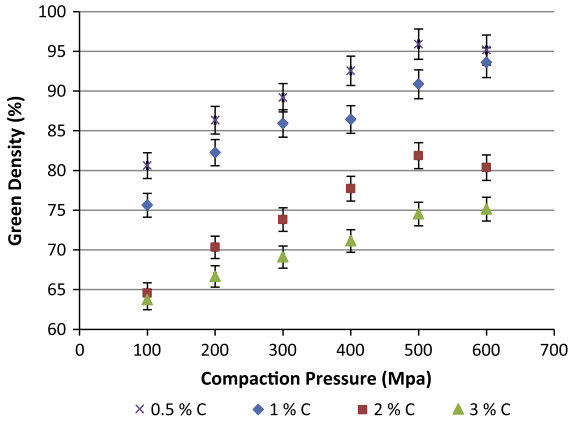

Fig. 3. Dependence of green density of alloys on carbon content and compaction pressure. (For interpretation of the references to colour in this figure legend, the reader is referred to the web version of this article.)

similar distributions of elements throughout the alloys (see Supplementary Information).

Parameters that affect the compressibility of an alloy include particle size, shape, distribution of elements, impurities, composition, added lubricant and hardening during mechanical alloying. It has been reported that both compaction pressure and sintering parameters influence the mechanical properties of sintered steels [10]. In this work, the compressibility of the alloys was determined by compacting them at pressures of 100, 200, 300, 400, 500 and 600 MPa and then measuring their green density according to a reported method [18]. The effects of compacting pressure and carbon content on the green density of the alloys are presented in Fig. 3. With increasing carbon content, deformation and work hardening of the powders reduce their compressibility, so the green density decreases correspondingly. This result is consistent with that reported previously for the relationship between carbon content and green density [19]. Compressibility curves generally show density saturation at high compaction pressures [18,20]. This is because the volume occupied by the powder prevents further

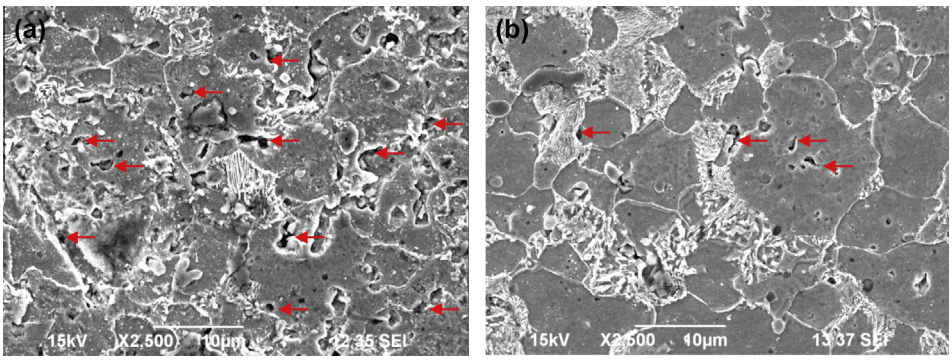

Fig. 4. Porosity of 0.5% C alloy compacted at a pressure of (a) 100 MPa and (b) 600 MPa.

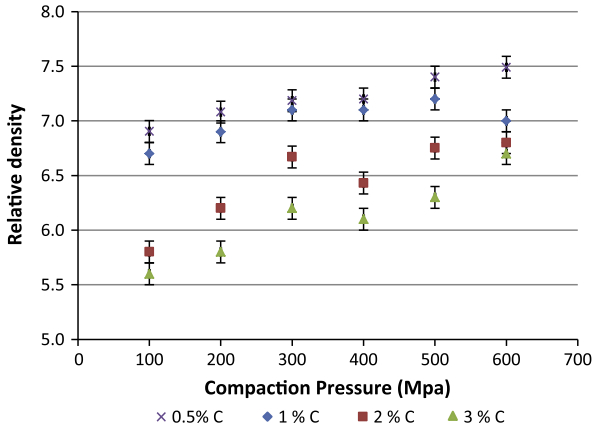

Fig. 5. Relative density of alloys containing different carbon contents following sintering.

densification of the compacted material at the upper saturation limit.

SEM images of the 0.5% C alloy compacted at different pressures are presented in Fig. 4. The morphology of the alloys depends on compaction pressure; as expected, those compacted at lower pressure have higher porosity. A similar dependence of porosity on compaction pressure was observed in SEM images of the other alloys (see Supplementary Information).

The compacted alloys with different carbon contents were then sintered. The relative density of the alloys increases following sintering, as shown in Fig. 5. During sintering, diffusion of atoms causes the contact area between particles to increase, which reduces porosity and correspondingly increases the density of the alloy. The densification achieved by sintering decreases with increasing carbon content of the alloy and decreasing compaction pressure.

SEM images of the sintered alloys containing different carbon contents that were compacted at 400 MPa are presented in Fig. 6.

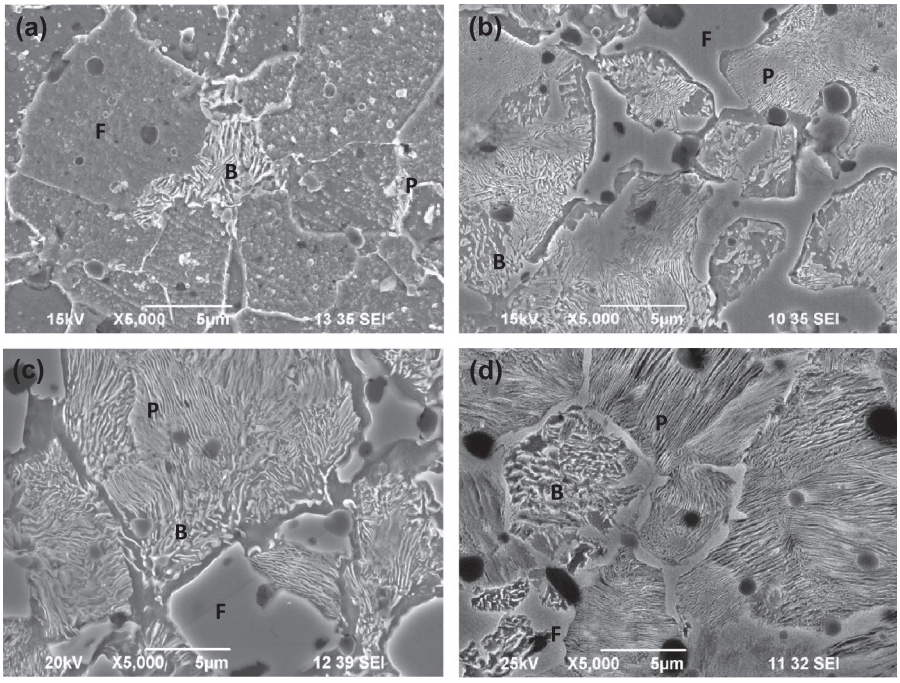

Fig. 6. SEM images of alloys sintered at 1200 °C containing (a) 0.5% C, (b) 1% C, (c) 2% C and (d) 3% C. P = pearlite, B = bainite, F = ferrite matrix.

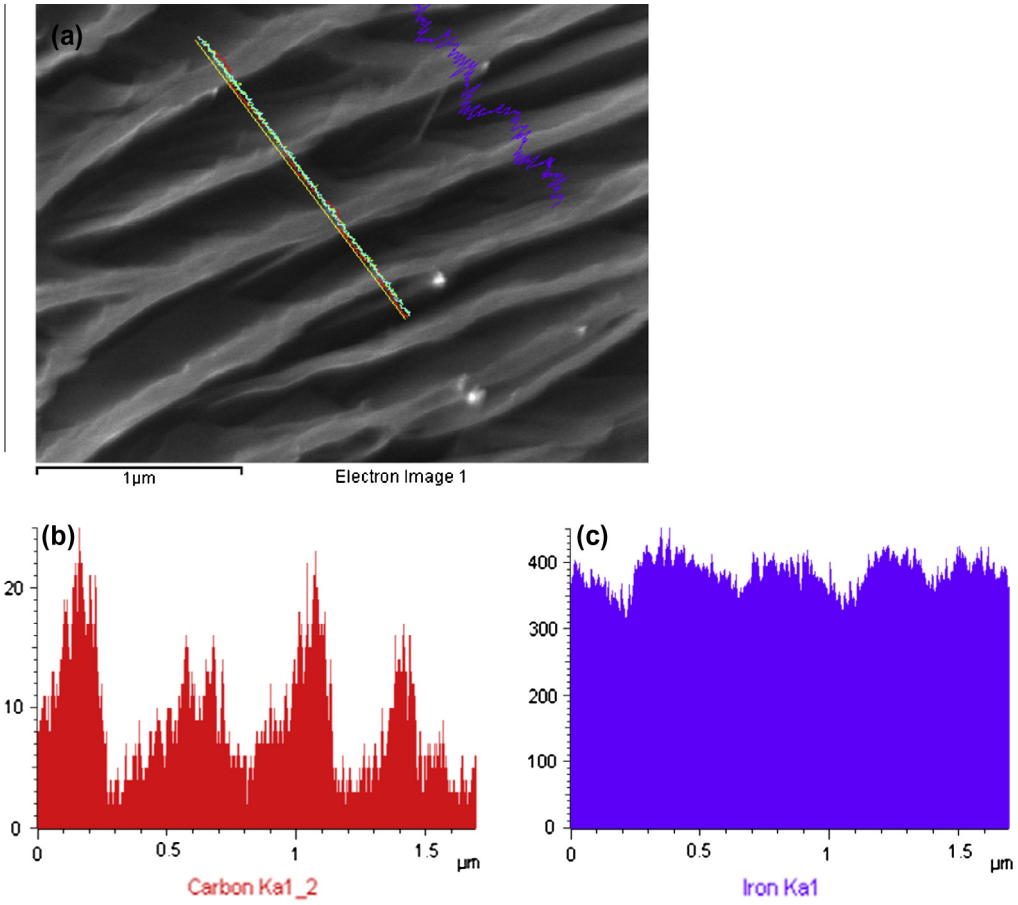

Fig. 7. (a) SEM image, and EDS microanalysis of (b) C and (c) Fe in a lamellar pearlite region in the 3% C alloy.

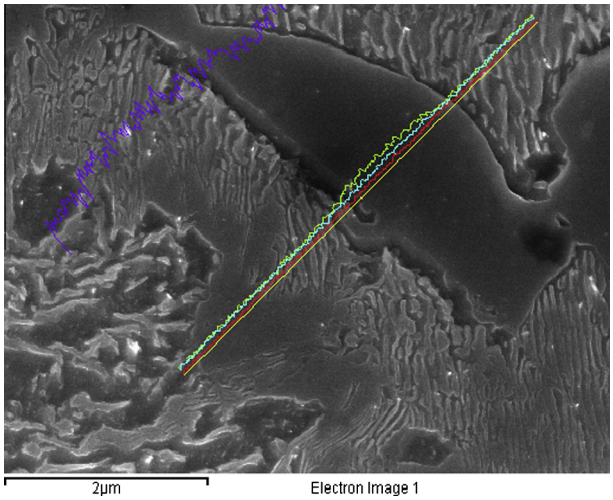

Fig. 8. SEM image at 10,000× of a region of the 3% C alloy with ferrite, cementite and a phase rich in C, Cr and Mn. EDS analysis of this area indicated it contained 7.6% C, 1.69% Cr and 1.27% Mn.

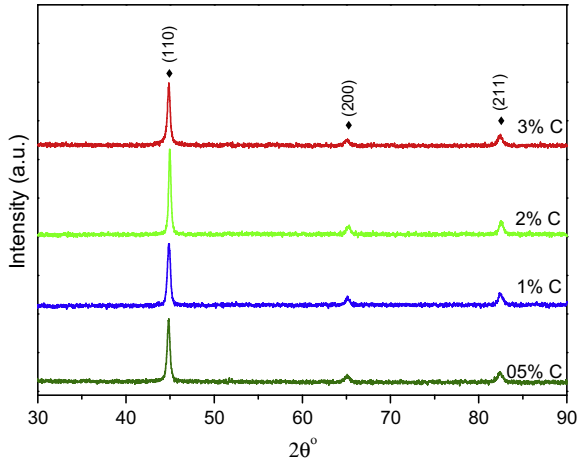

Fig. 9. XRD patterns of alloys containing different carbon contents.

Sintering induced the formation of pearlite and bainite regions in the ferritic matrix. Bainite is a non-lamellar aggregate of ferrite and cementite that is formed from the decomposition of austenite, and is generally more resistant to deformation and ductile than pearlite [21–23]. The formation of bainite has previously been correlated to a decrease in green density [24]. The regions of pearlite and bainite both increased with the carbon content of the alloys.

The dark areas in these images are attributed to residual carbon according to EDS measurements (see Supplementary Information). The number and size of residual carbon particles is proportional to the carbon content of the alloys. An SEM image and corresponding EDS microanalysis of the C and Fe in a pearlite region in the 3% C alloy are shown in Fig. 7, which clearly reveal the layers of ferrite and cementite. The 3% C alloy also contained particles rich in C, Cr and Mn. One such particle is illustrated in Fig. 8, where the interfaces between the phases can also be distinguished. We

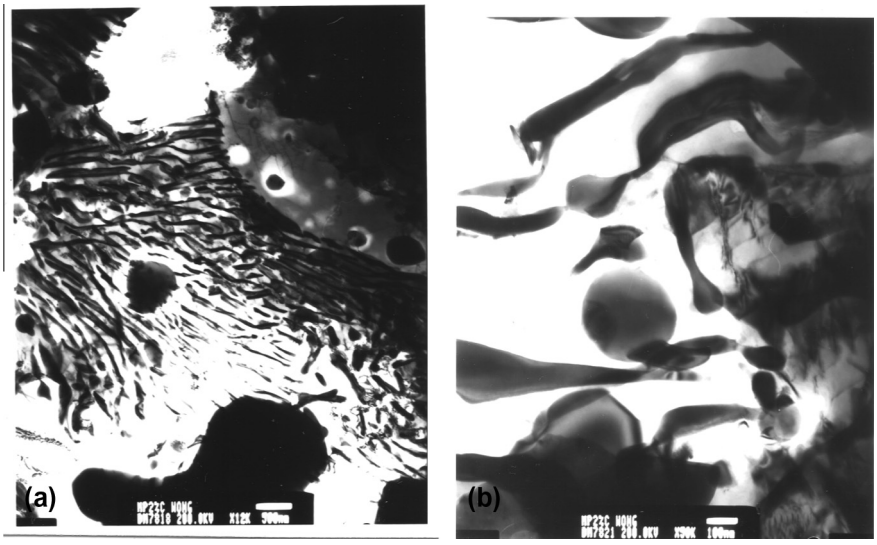

Fig. 10. Bright-field TEM images of the sintered sample with 2% C. (a) Pearlite microconstituent (left) and a ferrite grain both containing carbide particles. (b) A closer view of the pearlite microconstituent containing embedded carbide particles.

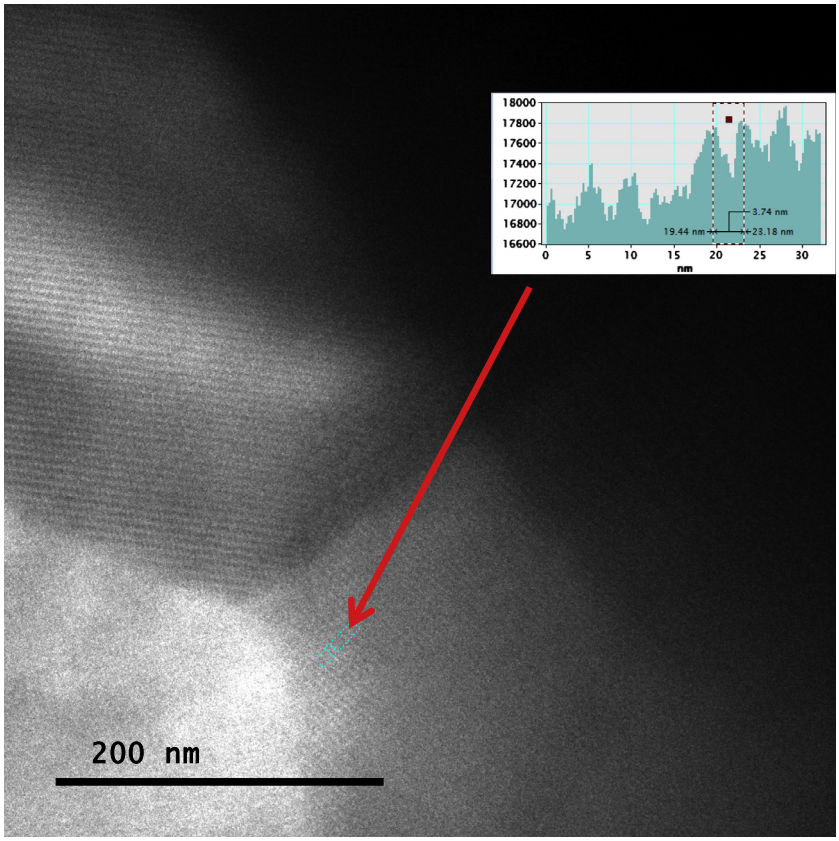

Fig. 11. HRTEM image and interplanar distance measurement of the sintered sample containing 2% C.

obtained powder XRD patterns of the samples to investigate their phase structure (Fig. 9). All of the reflections were consistent with ferrite; those of iron carbide were not observed.

Bright-field TEM images of the sintered sample containing 2% C are shown in Fig. 10. Fig. 10(a) depicts a pearlite microconstituent with a ferrite grain on the upper right side, both of which contain embedded carbide precipitates. Fig. 11 shows a digital HRTEM image of the sintered sample containing 2% C. An interphase boundary with different crystalline orientation at each side can be observed. An interplanar distance of 3.74 nm was determined by a line profile of the image, which corresponds to cementite particles.

The hardness of the alloys doped with different contents of carbon and compacted at different pressures is presented in Fig. 12. Maximum hardness is achieved following compaction at 400 MPa for the 0.5%, 2% and 3% C alloys, whereas that for the 1% C alloy

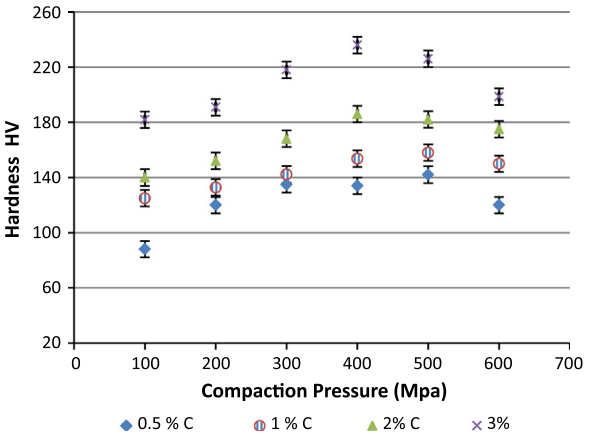

Fig. 12. Dependence of hardness of alloys on carbon content and compaction pressure.

is obtained for compaction at 500 MPa. The hardness of the alloys increases with carbon content. However, their hardness is relatively low compared with that of steel obtained by continuous casting [25]. In addition, the samples containing a larger content of carbon showed lower tenacity. Charpy tests revealed that the alloys containing 0.5%, 1%, 2% and 3% C possessed tenacities of 24, 20, 14 and 9 J, respectively. This means that as the hardness of the alloys increased, their ductility decreased, so they became more fragile. The results indicate that the microstructure, density and porosity of the alloys affect their hardness, which is consistent with the findings of Güral and Tekeli [24]. The hardness of the alloys may be improved by heat treatment after sintering.

4. Conclusions

Fe-based alloys were dopped with different contents of carbon to investigate its effect on the microstructure, density, hardness and ductility of the resulting materials. Alloys formed by ball milling elemental powders were compacted and then sintered. The alloys contained regions of pearlite and bainite in ferrite networks, which increased in size and number as the carbon content increased. The density of the alloys depended on both carbon content and compaction pressure; a higher pressure up to 500 MPa and lower carbon content gave a denser alloy. The hardness and ductility of the alloys also depended on both carbon content and compaction pressure. Alloys with a higher content of carbon and therefore more bainite were harder, but less ductile. The hardness of the alloys was lower than that of steel fabricated by continuous casting. These results show that PM can be used to form the resistant microstructure bainite in Fe-based alloys, which improved alloy hardness but reduced ductility as the amount of bainite increased.

Acknowledgments

The authors acknowledge support from the Instituto Politécnico Nacional de Mexico and Universidad Nacional Autónoma de Mexico (ESIQIE and IIM). We also thank the General Direction of Military Industry for providing elemental powder metallurgy samples and equipment.

Appendix A. Supplementary material

Supplementary data associated with this article can be found, in the online version, at http://dx.doi.org/10.1016/j.matdes.2014.04.039.

References

[1] Channankaiah RanganathG. Experimental approach on densification and mechanical properties of sintered powder metallurgy AISI 4140 steel preforms. J Eng Appl Sci 2012;7:298–303.
[2] Kandavel TK, Chandramouli R, Shanmugasundaram D. Experimental study of the plastic deformation and densification behaviour of some sintered low alloy P/M steels. Mater Des 2009;30:1768–76.
[3] Rochman NT, Kawamoto K, Sueyoshi H, Nakamura Y, Nishida T. Effect of milling temperature and additive elements on an Fe–C system alloy prepared by mechanical alloying. J Mater Process Technol 1999;89:367–72.
[4] German RM. Powder metallurgy and particulate processing. Princeton: Metal Powder Industries Federation; 2005.
[5] Bergman O, Bergmark A. Influence of microstructure on the fatigue performance of PM steels. Adv Powder Metall Part Mater 2003;7:270–8.
[6] Chawla N, Deng X. Microstructure and mechanical behavior of porous sintered steels. Mater Sci Eng A 2005;390:98–112.
[7] Li Y, Ngai T, Zhang D, Long Y, Xia W. Effect of die wall lubrication on warm compaction powder metallurgy. J Mater Process Technol 2002;129:354–8.
[8] Warke VS, Sisson Jr RD, Makhlouf M. Effect of porosity on the austenite to ferrite transformation in powder metallurgy steels. Mater Sci Eng A 2011;528:3533–8.
[9] Umemoto M, Liu ZG, Masuyama K, Hao XJ, Tsuchiya K. Nanostructured Fe–C alloys produced by ball milling. Scripta Mater 2001;44:1741–5.
[10] Shanmugasundaram D, Chandramouli R. Tensile and impact behaviour of sinter-forged Cr, Ni and Mo alloyed P/M steels. Mater Des 2009;30:3444–9.
[11] Hatami S, Malakizadi A, Nyborg L, Wallin D. Critical aspects of sinter-hardening of prealloyed Cr–Mo steel. J Mater Process Technol 2010;210:1180–9.
[12] Zuhailawati H. Microstructure and hardness characterization of mechanically alloyed Fe–C. Mater Des 2010;31:2211–5.
[13] Bensebaa N, Alleg S, Bentayeb FZ, Bessais L, Grenèche JM. Microstructural characterization of Fe–Cr–P–C powder mixture prepared by ball milling. J Alloys Compd 2005;388:41–8.
[14] Lonardellia I, Bortolotti M, Van Beek W, Girardini L, Zadra M, Bhadeshia HKDH. Powder metallurgical nanostructured medium carbon bainitic steel: kinetics, structure, and *in situ* thermal stability studies. Mater Sci Eng A 2012;555:139–47.
[15] Azadbeh M, Mohammadzadeh A, Danninger H. Modeling the response of physical and mechanical properties of Cr–Mo prealloyed sintered steels to key manufacturing parameters. Mater Des 2014;55:633–43.
[16] Materials Standard for PM Structural Parts Explanatory Notes and Definitions, Standard 42, Metal Powder Industries Federation; 2007.
[17] Arik H, Turker M. Production and characterization of in situ Fe–Fe_3C composite produced by mechanical alloying. Mater Des 2007;28:140–6.
[18] Davidson JE. In: Compressibility of metal powders. ASM Handbook, vol. 7. ASM International; 1993.
[19] Powder metal technologies and applications. ASM Handbook, vol. 7. ASM International; 1993.
[20] Höganäs Iron and steel powders for sintered components. Höganäs Handbook, Höganäs AB; 2002.
[21] Candela N, Velasco F, Martínez MA, Torralba J. Influence of microstructure on mechanical properties of molybdenum alloyed P/M steels. J Mater Process Technol 2005;168:505–10.
[22] Khorsand H, Habibi S, Yoozbashizadea H, Janghorban K, Reihani S, Rahmani H, et al. The role of heat treatment on wear behavior of powder metallurgy low alloy steels. Mater Des 2002;23:667–70.
[23] Molinari A. Advances in powder metallurgy and particulate materials. Princeton: Metal Powder Industries Federation; 2001.
[24] Güral A, Tekeli S. Microstructural characterization of intercritically annealed low alloy PM steels. Mater Des 2008;28:1224–30.
[25] Krauss G. Physical metallurgy and heat treatment of steel. In: Boyer HE, Gall TL, editors. Metals handbook desk edition. American Society for Metals; 1985. p. 28-2–28-10.